

## Energy spectrum and the shower maxima of cosmic rays above the knee region measured with the NICHE detectors at the TA site

---

**Yugo Omura,<sup>a,\*</sup> Ryosuke Tsuda,<sup>a</sup> Yoshiki Tsunesada,<sup>a</sup> Douglas R Bergman<sup>b</sup> and John F Krizmanic<sup>c</sup> on behalf of the Telescope Array Collaboration**  
(a complete list of authors can be found at the end of the proceedings)

<sup>a</sup>*Osaka City University, Graduate School of Science,  
Osaka, Japan*

<sup>b</sup>*The University of Utah, Department of Physics and Astronomy,  
Salt Lake City, Utah, USA*

<sup>c</sup>*University of Maryland, Baltimore County,  
Baltimore, Maryland, USA*

*E-mail: [omura@cosmicray-ocu.jp](mailto:omura@cosmicray-ocu.jp)*

The Non-Imaging Cherenkov (NICHE) Experiment is a low energy extension to Telescope Array (TA) using an array of closely spaced ( $\sim 100$  m) light collectors covering an area of  $\sim 2$  square km. It is being deployed in the field-of-view of the FD for the TA Low Energy Extension (TALE) and overlaps with the TALE FD in the energy range above 2 PeV. Cosmic ray air showers with energies 1–100 PeV will be reconstructed using the Lateral Distribution of Cherenkov light from the air showers. This method allows shower energy and the maximum of shower depth ( $X_{\max}$ ) to be determined. A prototype of the array, j-NICHE, has been making routine observations with 14 detectors since May, 2019. We will present the latest results of NICHE including the energy spectrum and the shower maximum distribution around the cosmic ray knee.

*37<sup>th</sup> International Cosmic Ray Conference (ICRC 2021)  
July 12th – 23rd, 2021  
Online – Berlin, Germany*

---

\*Presenter

## 1. Introduction

The mass composition of cosmic rays is very important for the clarification of their origin, because it must be strongly related to the sites of their origin, to the mechanisms of particle accelerations, and to the propagation from the sources to the Earth. There is a general agreement regarding cosmic ray composition that the fraction of the heavier component increases with energy around the knee region ( $E = 10^{15}$ – $10^{16}$  eV, see [7] for review). In air shower experiments, the types of the primary nuclei that induce air showers can be inferred from the longitudinal developments of the showers because both cross sections and first collision multiplicity increase with the mass of the primary cosmic nucleus interacting with the atmosphere. The results from the previous experiments show that the cosmic-ray mass  $\langle \ln A \rangle$  increases with energy, indicating a predominantly heavy composition at the knee. This is consistent with the rigidity-dependent stochastic particle acceleration models for cosmic ray sources. These models predict that the maximum reachable energy,  $E_{\max}$ , is proportional to the nuclear charge  $Z$ . On the other hand, it has been predicted that galactic cosmic ray sources such as supernovae cannot accelerate particles to energies greater than  $\sim 10^{18}$  eV. Thus we conclude that cosmic rays with such high energies are of extra-galactic origin. Protons and other lighter components would be dominant in this higher energy region, as heavier nuclei suffer from photo-disintegration in interactions with the cosmic microwave background (CMB) photons propagating over long distances. In fact, recent cosmic ray measurements in the ultra-high energy (UHE) region ( $E > 10^{18}$  eV), using the air fluorescence detection technique, show a proton-dominant composition at about  $10^{18}$  eV [1–3]. Therefore, we can expect a drastic change in the cosmic-ray mass composition in the energy range from  $10^{16}$  to  $10^{18}$  eV, *i.e.* from the heavier galactic components to the lighter extra-galactic components. The aim of the NICHE (Non-Imaging Cherenkov) experiment is to measure the mass composition of cosmic rays in this transition region.

## 2. NICHE at the TA site

A *Kakenhi* Grant by the Japan Society for the Promotion of Science (JSPS) was approved in 2014 for four years, and a prototype array of 14 air-Cherenkov detectors (CDs) has been developed. This array is called j-NICHE to distinguish it from other NICHE endeavors. The positions of the deployed j-NICHE counters are shown in the left panel of Figure 1. The detectors are deployed at  $\sim 800$  m away from the TA Middle Drum (MD) site with 100 m spacing to detect Cherenkov light generated by showers with  $E \geq 3 \times 10^{15}$  eV together with the MD and the TALE FDs.

A j-NICHE counter detects Cherenkov light using only one 3-inch photomultiplier tube (PMT, Hamamatsu R6233-100) whose output signal is digitized by an FADC (200MHz, 12 bits) and the resulting time series are stored in a micro-SD card. A Winston cone of opening half-angle  $45^\circ$  is attached above PMT to collect more inclined lights. They are made by machining a solid aluminum 4-inch dowel at the University of Utah. Ray tracing studies using ROBAST[9] (see our previous paper [10]) showed that photons with incident angle  $\theta \geq 43^\circ$  can not be seen by the PMT.

The housing for the j-NICHE counters includes a rotating platter with a hole that serves as a shutter that protects the PMT and Winston cone from Sunlight. The housing also contains the batteries as well as data acquisition and control electronics. While the current prototype deploys a

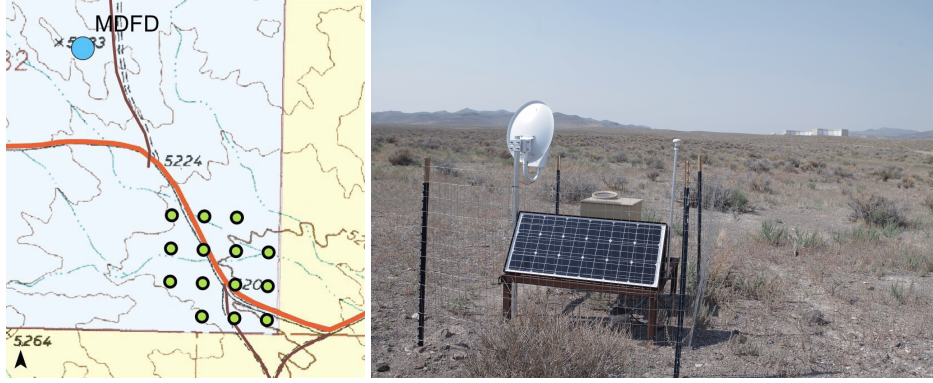


**Figure 1:** Left: The map around the TA Middle Drum (MD) site. The j-NICHE counters denoted by green circles are deployed with 100 m spacing  $\sim 800$  m away from the MD site. Right: A j-NICHE counter in the field with MD-FD behind.

First Quality Criterion	Second Quality Criterion
Zenith angle $< 30^\circ$	Use of the smallest 95% of $\chi^2$ dist.
Good progress on optimization	
The number of detectors $\geq 5$	
Core distance from the center of the array $R_p < 200$ m	

**Table 1:** Quality criteria for MC simulation/observation data. For  $X_{\max}$  determination, we use the more strict first criterion: the number of detectors  $\geq 6$  and  $R_p < 100$  m.

single PMT per detector, a two-PMT design for future NICHE hybrid array will allow for a local coincidence trigger and thus a lower threshold and/or a lower trigger rate.

### 3. Observation data

In this paper, we use the observation data for one year between March 2019 and March 2020. The total observation time is 536.9 hours and the total number of recorded shower events is 165,839. Finally, there are 4,943 events left by the data cleansing (Table 1) after the following correction.

#### 3.1 Calibration using NICHE-TALE hybrid events

We extend a technique of TALE FD-SD hybrid analysis [8] for NICHE detectors and TALE-FD to calibrate NICHE detectors by comparing observed NICHE signals to those estimated from the lateral distribution function (Equation 1) based on the result of the hybrid analysis with TALE FD that included 453 events for the 28 day period with the longest operation time in 2019.

### 4. Monte-Carlo simulation

5,042 showers are generated using CORSIKA[6] and each shower is resampled 980/1,280/2,000 times by changing core position uniformly on the observation level. The detail of CORSIKA simulation is shown in Table 2.

Particle type	Proton/Iron
Limit of zenith angle	0 - 40°
Limit of core position	-500m < X/Y < 500m
High-energy hadronic interaction model	QGSJETII-04
Low-energy hadronic interaction model	GHEISHA
Thinning	No
Maximum bunch size of Cherenkov photons	1

**Table 2:** CORSIKA options

For comparison between the MC simulation and the real data, we resampled the original CORSIKA showers, assuming uniform core position along  $X$  (east to west) or  $Y$  (south to north) and according to a differential power law energy distribution ( $\propto E^{-3}$ ). In the resampling, events were randomly chosen with replacement, from the original showers in order to maintain the proper phase-space distributions of zenith angles and to maintain the correct apparent detector effective area ( $\propto \sin\theta\cos\theta$ ). This procedure produced about ten million events.

From the generated shower, we perform ray-tracing of all photons passing through a larger-than-required effective area defined for each detector, to the PMT, possibly reflecting off the inner side of the Winston cone[10]. After hitting the PMT cathode, the impulse response, the transit time of the PMT and, self-triggering of the electronics are simulated and recorded.

#### 4.1 Reconstruction method

We have developed reconstruction methods based on examinations of the simulation result. The steps are similar to those for the standard reconstruction of air showers using a surface detector array.

Shower arrival directions are determined by fitting photon arrival times with a shower plane propagating at the speed of light in air. To select properly reconstructed events, we required each event to have at least five hit detectors, and a core distance  $R_c < 100$  m, where  $R_c$  is the distance from the center of the NICHE array to shower axis. Our results show that 68% of CORSIKA showers are reconstructed within  $0.94^\circ$  of their thrown (*i.e.* true) directions (Figure 4).

Core positions of showers are determined by searching the positions on the shower planes that minimize the weighted Mean Squared Error (MSE) of the photon signal from the expectation of the Lateral Distribution Function (LDF). For this process, we use the modified LDF of the Tunka-Experiments One[5], shown in equation 1.

$$Q(R; Q_{200}, R_{kn}, R_0, b_2, b_Q) = \begin{cases} Q_{200} \cdot \left(\frac{200}{R_{kn}}\right)^{b_2} \cdot \exp\left(-\sqrt{\frac{R}{R_0}} + \sqrt{\frac{R_{kn}}{R_0}}\right) & R \leq R_{kn} \\ Q_{200} \cdot \left(\frac{200}{R}\right)^{b_2} & R_{kn} \leq R \leq 300\text{m} \\ Q_{200} \cdot \left(\frac{2}{3}\right)^{b_2} \cdot \left(\left(\frac{R}{300} + 1\right)/2\right)^{-b_Q} & R > 300\text{m} \end{cases} \quad (1)$$

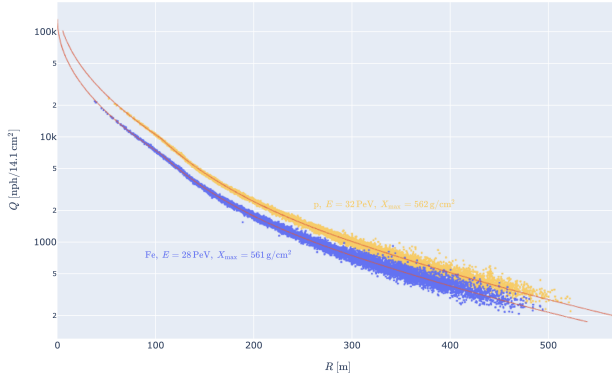


**Figure 2:** Typical examples of LDF fitting all data points detected on NICHE detectors for one CORSIKA shower resampled 980 times by varying core positions.

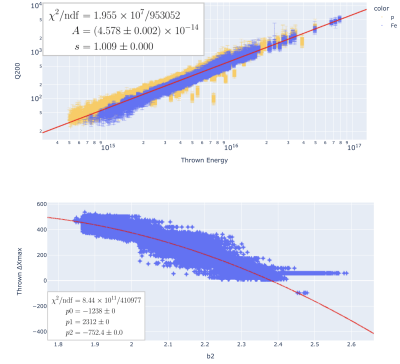


**Figure 3:** LDF-parameters vs energy (upper) or  $\Delta X_{\max}$  (lower) for all data points from the same resampling showers as performed for Figure 2.

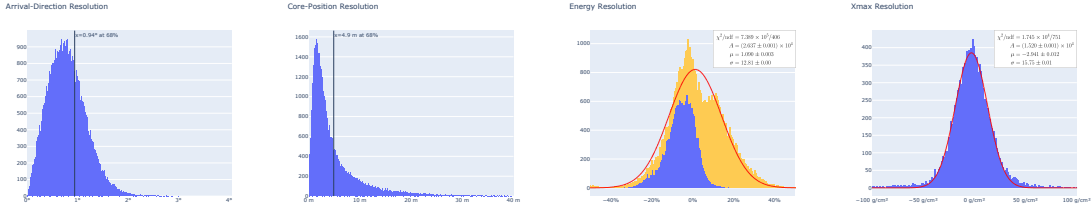


**Figure 4:** Resolutions at 6 PeV of arrival direction, core position, energy and  $X_{\max}$ .

The typical examples of LDF is shown in Figure 2. The core-position distribution in Figure 4 shows that 68% of simulated showers are reconstructed within 4.9 m of their thrown core locations.

LDF parameters  $Q_{200}$  and  $b_2$  appear tightly correlated to shower energy and  $\Delta X_{\max}$  respectively, where  $\Delta X_{\max}$  is the thickness between the observation level and the air-shower maximum depth. These relationships are illustrated in Figure 3.

For estimation of energy and  $X_{\max}$ , the optimization problem is solved by minimizing the weighted MSE of detected signals from the expectations of the LDF by varying four free parameters: core positions  $X$  and  $Y$  on the shower plane, and LDF parameters  $Q_{200}$  and  $b_2$ . The distributions of reconstruction errors of energy and  $X_{\max}$  for simulated events are shown in Figure 4. These distributions give a reconstruction RMS error of 12.8% in energy and 15.75 g/cm<sup>2</sup> in  $X_{\max}$ .

## 4.2 Comparison between MC simulation and observation data

To evaluate how much my MC simulation reflects the real process, we compare my MC simulation to the observation data in five parameters: zenith angle, azimuthal angle, number (N-fold) of hit detectors, energy, and  $X_{\max}$ . These are plotted in Figure 5, which shows good agreement between the data distributions of zenith, azimuth, and  $X_{\max}$  to those from simulation if one assume a mixed composition. The mismatch seen in the number of hit detectors and energy may be indications of a mismatch in the trigger or reconstruction thresholds between data and MC.

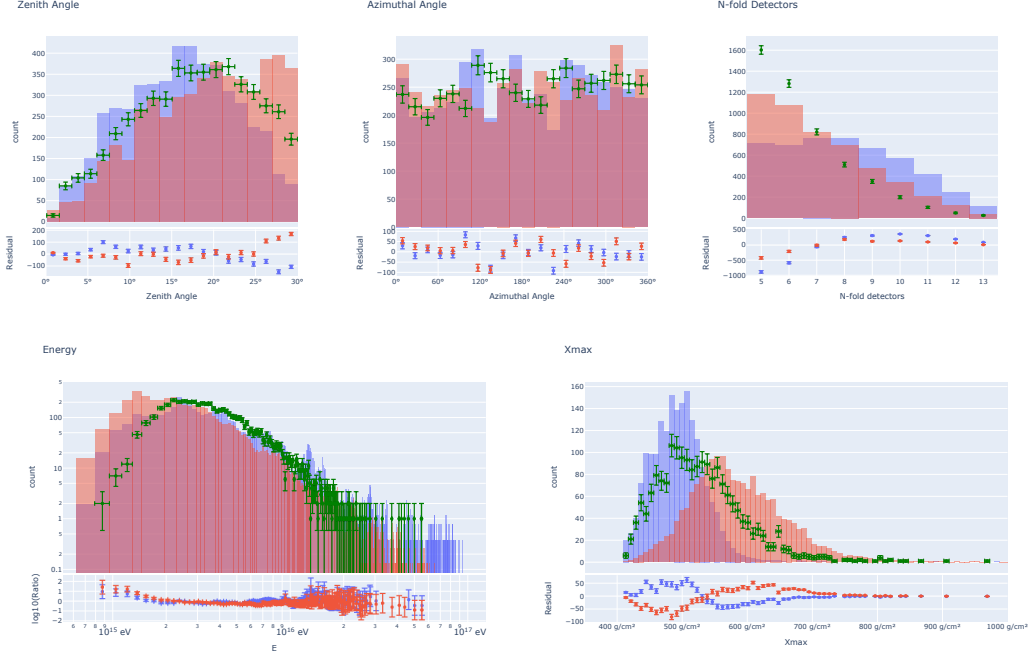


**Figure 5:** Data distributions overlaid with MC predictions, normalized to the number of data event, for (starting from top left to the right) zenith angle, azimuthal angle, number of hit detector, log of energy, and  $X_{\max}$ . Green data points show the observation data. Red and blue histograms show the simulated distributions for the proton and iron showers, respectively.

### 4.3 Aperture

The detector aperture is given as follows[4]:

$$A(E, t) = \int \epsilon(E, t, \theta, \phi, x, y) \cos\theta dS d\Omega \quad (2)$$

where  $\epsilon$  is the detection efficiency including self-triggering, reconstruction and the data cleansing,  $t$  is the exposure time, which depends on the actual detector configuration during the one year observation period,  $dS$  is the area on the observation level and  $d\Omega = \sin\theta d\theta d\phi$  is the differential solid angle.

In this paper, we assume that  $\epsilon$  is independent of  $t$ ,  $\theta$ ,  $\phi$ ,  $x$  and  $y$ , so that for sufficiently large  $N$  and  $S_{\max}$ , the aperture is approximates to

$$A(E) \approx \frac{\pi}{4} \cdot \frac{N_{\text{sel}}(E)}{N(E)} \cdot S_{\max} \quad (3)$$

where  $N_{\text{sel}}(E, t)$  is the number of the reconstructed events passing the quality criteria (Table 1),  $S_{\max}$  is the area of the events thrown uniformly along both X and Y of core positions on the observation level and  $N$  is the number of thrown events. The aperture as given in Equation 3 is calculated separately for each energy bin and the result is shown in Figure 6.

We note that  $\epsilon$  does actually depend on  $t$  because the combination of available detectors changes with time, so we will account for this effect in the future.

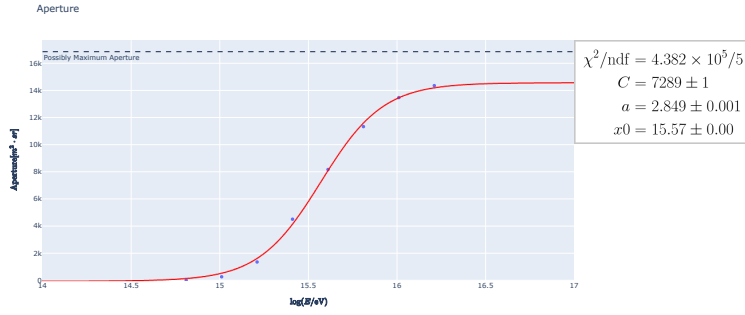


**Figure 6:** NICHE aperture in the case that all 13 detectors are available. The red solid line is a rescaled hyperbolic tangent function (*i.e.* a logistic sigmoid) fit to the simulation results.

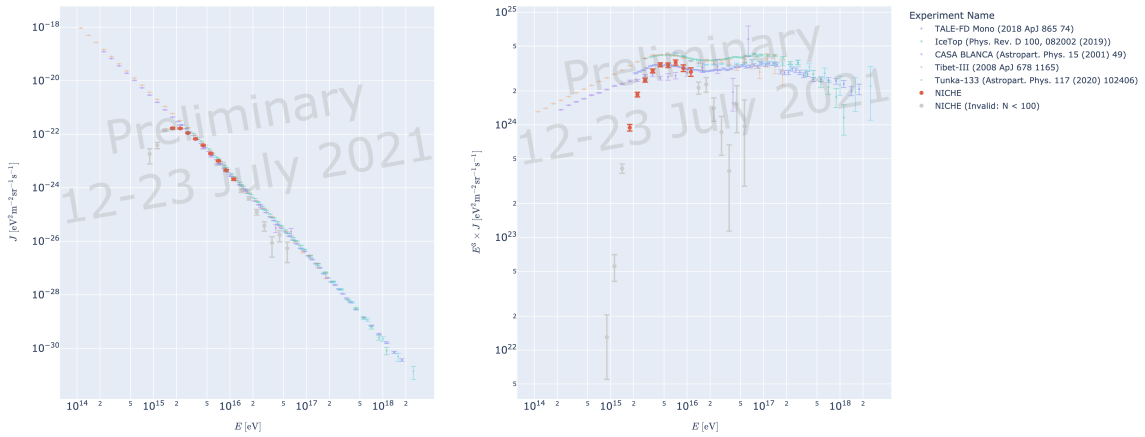


**Figure 7:** Energy spectrum measured by jNICHE, overlaid with those of other experiments. Left: The flux function  $J(E)$ . Right:  $E^3 J(E)$ , the flux multiplied by  $E^3$  to flatten the curve.

## 5. Energy spectrum and mass composition

To calculate the uncorrected flux  $J_{uc}$ , we divide the number of events inside each energy bin by the linear bin width  $\Delta E$  (the distributions are binned in  $\log E$ , with  $\log E = 0.1$ ), the aperture calculated above, and the total observation time. We then apply the correction of bin-to-bin-event-migration to  $J_{uc}$  which depends on the energy resolution shown in Figure 4 to unfold then spectrum. The resulting NICHE preliminary energy spectrum for one year of observation is shown in Figure 7. At the lower limit, the NICHE energy spectrum appears underestimated when compared with the results of other measurements. This is consistent with the hypothesis of a mismatch of thresholds between data and MC that led to the discrepancy seen in the comparisons of number of hit detectors and of energy in Figure 5.

For a mass-composition analysis, we use the  $X_{max}$  distribution in each energy bin to calculate its mean,  $\langle X_{max} \rangle$ , the value of  $\ln A$  is then extracted for each bin by scaling between the simulated proton ( $\ln A = 0$ ) and iron ( $\ln A \sim 4$ ) rails, and plotted against  $\log E$  (Figure 8). The resulting NICHE preliminary "elongation plot" shows a composition that is getting heavier with increasing energy



**Figure 8:** Top left:  $X_{\max}$  distributions for different eight energy bins. Bottom left: Scatter plot of  $X_{\max}$  vs  $\log E$  (*i.e.* the "elongation plot"). Right: Scatter plot of  $\ln A$  vs  $\log E$  overlaid with results of other experiments.

up to almost pure iron at  $\sim 10^{16}$  eV.

## 6. Summary

The goal of the NICHE experiment is to measure the cosmic-ray composition between  $10^{16}$  and  $10^{18}$  eV by measuring Cherenkov light generated by air-showers using 14 detectors placed in a grid of 100 m spacing. The preliminary NICHE results of the energy spectrum and mass composition have been presented.

## References

- [1] R.U. Abbasi et al. *Phys. Rev. Lett.*, 104:161101, 2010.
- [2] R.U. Abbasi et al. *Astropart. Phys.*, 64:49–62, 2015.
- [3] J. Abraham et al. *Phys. Rev. Lett.*, 104:091101–1–7, 2010.
- [4] P. Abreu et al. *Astropart. Phys.*, 34:368–381, 2011.
- [5] N.M. Budnev et al. *Astropart. Phys.*, 117:102406, 2020.
- [6] D. Heck, J. Knapp, J.N. Capdevielle, et al. *Report FZKA 6019, Forschungszentrum, Karlsruhe*, 1998.
- [7] Karl-Heinz Kampert and Michael Unger. *Astropart. Phys.*, 35:660, 2012.
- [8] S. Ogio. *PoS, ICRC2019:375*, 2019.
- [9] Akira Okumura, Koji Noda, and Cameron Rulten. *Astropart. Phys.*, 76:2016, 38.
- [10] Yugo Omura, Kei Nakai, Yoshiki Tsunesada, Douglas R Bergman, and John F Krizmanic. *PoS, ICRC2019:379*, 2019.

**Full Authors List: Telescope Array Collaboration**

R.U. Abbasi<sup>1,2</sup>, T. Abu-Zayyad<sup>1,2</sup>, M. Allen<sup>2</sup>, Y. Arai<sup>3</sup>, R. Arimura<sup>3</sup>, E. Barcikowski<sup>2</sup>, J.W. Belz<sup>2</sup>, D.R. Bergman<sup>2</sup>, S.A. Blake<sup>2</sup>, I. Buckland<sup>2</sup>, R. Cady<sup>2</sup>, B.G. Cheon<sup>4</sup>, J. Chiba<sup>5</sup>, M. Chikawa<sup>6</sup>, T. Fujii<sup>7</sup>, K. Fujisue<sup>6</sup>, K. Fujita<sup>3</sup>, R. Fujiwara<sup>3</sup>, M. Fukushima<sup>6</sup>, R. Fukushima<sup>3</sup>, G. Furlich<sup>2</sup>, R. Gonzalez<sup>2</sup>, W. Hanlon<sup>2</sup>, M. Hayashi<sup>8</sup>, N. Hayashida<sup>9</sup>, K. Hibino<sup>9</sup>, R. Higuchi<sup>6</sup>, K. Honda<sup>10</sup>, D. Ikeda<sup>9</sup>, T. Inadomi<sup>11</sup>, N. Inoue<sup>12</sup>, T. Ishii<sup>10</sup>, H. Ito<sup>13</sup>, D. Ivanov<sup>2</sup>, H. Iwakura<sup>11</sup>, A. Iwasaki<sup>3</sup>, H.M. Jeong<sup>14</sup>, S. Jeong<sup>14</sup>, C.C.H. Jui<sup>2</sup>, K. Kadota<sup>15</sup>, F. Kakimoto<sup>9</sup>, O. Kalashev<sup>16</sup>, K. Kasahara<sup>17</sup>, S. Kasami<sup>18</sup>, H. Kawai<sup>19</sup>, S. Kawakami<sup>3</sup>, S. Kawana<sup>12</sup>, K. Kawata<sup>6</sup>, I. Kharuk<sup>16</sup>, E. Kido<sup>13</sup>, H.B. Kim<sup>4</sup>, J.H. Kim<sup>2</sup>, J.H. Kim<sup>2</sup>, M.H. Kim<sup>14</sup>, S.W. Kim<sup>14</sup>, Y. Kimura<sup>3</sup>, S. Kishigami<sup>3</sup>, Y. Kubota<sup>11</sup>, S. Kurisu<sup>11</sup>, V. Kuzmin<sup>16\*</sup>, M. Kuznetsov<sup>16,20</sup>, Y.J. Kwon<sup>21</sup>, K.H. Lee<sup>14</sup>, B. Lubsandorzhiiev<sup>16</sup>, J.P. Lundquist<sup>2,22</sup>, K. Machida<sup>10</sup>, H. Matsumiya<sup>3</sup>, T. Matsuyama<sup>3</sup>, J.N. Matthews<sup>2</sup>, R. Mayta<sup>3</sup>, M. Minamino<sup>3</sup>, K. Mukai<sup>10</sup>, I. Myers<sup>2</sup>, S. Nagataki<sup>13</sup>, K. Nakai<sup>3</sup>, R. Nakamura<sup>11</sup>, T. Nakamura<sup>23</sup>, T. Nakamura<sup>11</sup>, Y. Nakamura<sup>11</sup>, A. Nakazawa<sup>11</sup>, E. Nishio<sup>18</sup>, T. Nonaka<sup>6</sup>, H. Oda<sup>3</sup>, S. Ogio<sup>3,24</sup>, M. Ohnishi<sup>6</sup>, H. Ohoka<sup>6</sup>, Y. Oku<sup>18</sup>, T. Okuda<sup>25</sup>, Y. Omura<sup>3</sup>, M. Ono<sup>13</sup>, R. Onogi<sup>3</sup>, A. Oshima<sup>3</sup>, S. Ozawa<sup>26</sup>, I.H. Park<sup>14</sup>, M. Potts<sup>2</sup>, M.S. Pshirkov<sup>16,27</sup>, J. Remington<sup>2</sup>, D.C. Rodriguez<sup>2</sup>, G.I. Rubtsov<sup>16</sup>, D. Ryu<sup>28</sup>, H. Sagawa<sup>6</sup>, R. Sahara<sup>3</sup>, Y. Saito<sup>11</sup>, N. Sakaki<sup>6</sup>, T. Sako<sup>6</sup>, N. Sakurai<sup>3</sup>, K. Sano<sup>11</sup>, K. Sato<sup>3</sup>, T. Seki<sup>11</sup>, K. Sekino<sup>6</sup>, P.D. Shah<sup>2</sup>, Y. Shibasaki<sup>11</sup>, F. Shibata<sup>10</sup>, N. Shibata<sup>18</sup>, T. Shibata<sup>6</sup>, H. Shimodaira<sup>6</sup>, B.K. Shin<sup>28</sup>, H.S. Shin<sup>6</sup>, D. Shinto<sup>18</sup>, J.D. Smith<sup>2</sup>, P. Sokolsky<sup>2</sup>, N. Sone<sup>11</sup>, B.T. Stokes<sup>2</sup>, T.A. Stroman<sup>2</sup>, Y. Takagi<sup>3</sup>, Y. Takahashi<sup>3</sup>, M. Takamura<sup>5</sup>, M. Takeda<sup>6</sup>, R. Takeishi<sup>6</sup>, A. Taketa<sup>29</sup>, M. Takita<sup>6</sup>, Y. Tameda<sup>18</sup>, H. Tanaka<sup>3</sup>, K. Tanaka<sup>30</sup>, M. Tanaka<sup>31</sup>, Y. Tanoue<sup>3</sup>, S.B. Thomas<sup>2</sup>, G.B. Thomson<sup>2</sup>, P. Tinyakov<sup>16,20</sup>, I. Tkachev<sup>16</sup>, H. Tokuno<sup>32</sup>, T. Tomida<sup>11</sup>, S. Troitsky<sup>16</sup>, R. Tsuda<sup>3</sup>, Y. Tsunesada<sup>3,24</sup>, Y. Uchihori<sup>33</sup>, S. Udo<sup>9</sup>, T. Uehama<sup>11</sup>, F. Urban<sup>34</sup>, T. Wong<sup>2</sup>, K. Yada<sup>6</sup>, M. Yamamoto<sup>11</sup>, K. Yamazaki<sup>9</sup>, J. Yang<sup>35</sup>, K. Yashiro<sup>5</sup>, F. Yoshida<sup>18</sup>, Y. Yoshioka<sup>11</sup>, Y. Zhezher<sup>6,16</sup>, and Z. Zundel<sup>2</sup>

<sup>1</sup> Department of Physics, Loyola University Chicago, Chicago, Illinois, USA

<sup>2</sup> High Energy Astrophysics Institute and Department of Physics and Astronomy, University of Utah, Salt Lake City, Utah, USA

<sup>3</sup> Graduate School of Science, Osaka City University, Osaka, Osaka, Japan

<sup>4</sup> Department of Physics and The Research Institute of Natural Science, Hanyang University, Seongdong-gu, Seoul, Korea

<sup>5</sup> Department of Physics, Tokyo University of Science, Noda, Chiba, Japan

<sup>6</sup> Institute for Cosmic Ray Research, University of Tokyo, Kashiwa, Chiba, Japan

<sup>7</sup> The Hakubi Center for Advanced Research and Graduate School of Science, Kyoto University, Kitashirakawa-Oiwakecho, Sakyo-ku, Kyoto, Japan

<sup>8</sup> Information Engineering Graduate School of Science and Technology, Shinshu University, Nagano, Nagano, Japan

<sup>9</sup> Faculty of Engineering, Kanagawa University, Yokohama, Kanagawa, Japan

<sup>10</sup> Interdisciplinary Graduate School of Medicine and Engineering, University of Yamanashi, Kofu, Yamanashi, Japan

<sup>11</sup> Academic Assembly School of Science and Technology Institute of Engineering, Shinshu University, Nagano, Nagano, Japan

<sup>12</sup> The Graduate School of Science and Engineering, Saitama University, Saitama, Saitama, Japan

<sup>13</sup> Astrophysical Big Bang Laboratory, RIKEN, Wako, Saitama, Japan

<sup>14</sup> Department of Physics, SungKyunKwan University, Jang-an-gu, Suwon, Korea

<sup>15</sup> Department of Physics, Tokyo City University, Setagaya-ku, Tokyo, Japan

<sup>16</sup> Institute for Nuclear Research of the Russian Academy of Sciences, Moscow, Russia

<sup>17</sup> Faculty of Systems Engineering and Science, Shibaura Institute of Technology, Minato-ku, Tokyo, Japan

<sup>18</sup> Department of Engineering Science, Faculty of Engineering, Osaka Electro-Communication University, Neyagawa-shi, Osaka, Japan

<sup>19</sup> Department of Physics, Chiba University, Chiba, Chiba, Japan

<sup>20</sup> Service de Physique Théorique Université Libre de Bruxelles, Brussels, Belgium

<sup>21</sup> Department of Physics, Yonsei University, Seodaemun-gu, Seoul, Korea

<sup>22</sup> Center for Astrophysics and Cosmology, University of Nova Gorica, Nova Gorica, Slovenia

<sup>23</sup> Faculty of Science, Kochi University, Kochi, Kochi, Japan

<sup>24</sup> Nambu Yoichiro Institute of Theoretical and Experimental Physics, Osaka City University, Osaka, Osaka, Japan

<sup>25</sup> Department of Physical Sciences, Ritsumeikan University, Kusatsu, Shiga, Japan

<sup>26</sup> Quantum ICT Advanced Development Center, National Institute for Information and Communications Technology, Koganei, Tokyo, Japan

<sup>27</sup> Sternberg Astronomical Institute, Moscow M.V. Lomonosov State University, Moscow, Russia

<sup>28</sup> Department of Physics, School of Natural Sciences, Ulsan National Institute of Science and Technology, UNIST-gil, Ulsan, Korea

<sup>29</sup> Earthquake Research Institute, University of Tokyo, Bunkyo-ku, Tokyo, Japan

<sup>30</sup> Graduate School of Information Sciences, Hiroshima City University, Hiroshima, Hiroshima, Japan

<sup>31</sup> Institute of Particle and Nuclear Studies, KEK, Tsukuba, Ibaraki, Japan

<sup>32</sup> Graduate School of Science and Engineering, Tokyo Institute of Technology, Meguro, Tokyo, Japan

<sup>33</sup> Department of Research Planning and Promotion, Quantum Medical Science Directorate, National Institutes for Quantum and Radiological Science and Technology, Chiba, Chiba, Japan

<sup>34</sup> CEICO, Institute of Physics, Czech Academy of Sciences, Prague, Czech Republic

<sup>35</sup> Department of Physics and Institute for the Early Universe, Ewha Womans University, Seodaemun-gu, Seoul, Korea